Biointerphases

RESEARCH ARTICLE | SEPTEMBER 05 2024

Influence of metal oxides on biocompatibility of additively manufactured NiTi

Maria P. Kwesiga; Roger J. Guillory, II; Ali Gökhan Demir

Biointerphases 19, 051001 (2024)
https://doi.org/10.1116/6.0003665

Biointerphases
A Journal of Biomaterials and Biological Interfaces

ARTICLE

pubs.aip.org/avs/bip

Influence of metal oxides on biocompatibility of additively manufactured NiTi

Cite as: Biointerphases 19, 051001 (2024); doi: 10.1116/6.0003665
Submitted: 4 April 2024 · Accepted: 7 August 2024 ·
Published Online: 5 September 2024

Maria P. Kwesiga,[1] Roger J. Guillory, II,[2] and Ali Gökhan Demir[3,a)]

AFFILIATIONS

[1]Department of Biomedical Sciences, Grand Valley State University, Allendale, Michigan, 49401, USA
[2]Joint Department of Biomedical Engineering, Medical College of Wisconsin, Marquette University, Milwaukee, Wisconsin, 53226, USA
[3]Department of Mechanical Engineering, Politecnico di Milano, Via La Masa 1, 20156 Milan, Italy

[a)]**Author to whom correspondence should be addressed:** aligokhan.demir@polimi.it

ABSTRACT

In order to properly satisfy biomedical constraints for cardiovascular applications, additively manufactured NiTi scaffolds required further process and metallurgical engineering. Additively manufactured NiTi materials for cardiovascular use will have to undergo surface finishing in order to minimize negative surface interactions within the artery. In this study, we sought to understand biocompatibility from chemically etched additively manufactured NiTi scaffolds by laser powder bed fusion (LPBF). Although two distinct oxide films were created in the surface etching process (labeled CP-A and CP-B), no qualitative changes in microroughness were seen between the two conditions. CP-A possessed significantly less Ni at the surface (0.19 at. %) than the CP-B group (3.30 at. %), via x-ray photoelectron spectroscopy, alongside a concomitant shift in the O1 s peak presentation alluding to a greater formation of a Ni based oxide in the CP-B group. Our live dead staining revealed significant toxicity and reduced cellular attachment for the CP-B group, in addition to inducing more cell lysis (20.9 ± 5.1%), which was significantly increased when compared to CP-A ($P < 0.01$). Future practices of manufacturing NiTi scaffolds using LPBF should focus on producing surface films that are not only smooth, but free of cytotoxic Ni based oxides.

I. INTRODUCTION

In the past 10 years, additive manufacturing of nickel-titanium (NiTi) based materials for biomedical applications has rapidly developed.[1] Using this unique manufacturing style is attractive for biomedical applications, and the possibility of creating patient specific implants grows more attractive as clinical imaging and feature extraction becomes more robust and readily available.[2] To date, significant focus has been placed on using these structures for orthopedic load bearing applications such as fracture fixation devices, spinal rods, and orthodontic arch wires.[3] Creating scaffolds with reduced stiffness in order to remedy the stress shielding affect produced by load bearing orthopedic implants with modulus values greater than 10 times that of bone has been a biomedical engineering topic matter for the past 20 years.[4,5] Additionally, conventionally manufactured NiTi has been used for a variety of cardiovascular applications such as self-expanding stents,[6] vena cava filters,[7] and graft scaffolding.[8] Only recently has additively manufactured NiTi scaffolds been considered for cardiovascular applications.[9,10]

In order to properly satisfy biomedical constraints for cardiovascular applications, additively manufactured NiTi scaffolds required further process and metallurgical engineering. Current on market cardiovascular NiTi devices are primarily used due to their (1) fine-tuned shape memory effect, (2) super elasticity and self-expandability, and (3) inert passive behavior within the artery.[11] While there has been significant research performed on engineering points 1 and 2, minimal evidence has been presented to date that shows extensive biocompatibility of these scaffolds. For arterial use, it is critical that the scaffold is smooth and does not corrode/leach Ni over the implantation period.[12]

Currently, NiTi stents undergo surface finishing steps such as sand blasting, electropolishing, or chemical etching before final catheter crimping and sterilization.[13] The polishing step reduces stent roughness, improves corrosion behavior, and rids the surface of all processing contaminates.[14] Additively manufactured NiTi materials for cardiovascular use will have to undergo surface finishing in order to minimize negative surface interactions within the

artery.[15] Principally, a homogeneous TiO_2 layer with minimal Ni is preferred for optimal biocompatibility.[16] In this study, we sought to understand the biocompatibility from chemically etched additively manufactured NiTi scaffolds by laser powder bed fusion (LPBF). We have evaluated the surface oxide features using XPS to track critical oxide formations. We then compared the biocompatibility response to a commercial NiTi stent, across multiple cell types.

II. MATERIALS AND METHODS

A. Materials

The NiTi powder was produced through gas atomization and its nominal chemical composition was $Ni_{50.8}Ti_{49.2}$ (SAES Getters SpA, Lainate, Italy). Impurities were kept below 605 ppm C and 1254 ppm O. The nominal particle size distribution was 15–53 μm (D10–D90). The powder had an austenite finish temperature (A_f) of 16 °C. Samples were produced on NiTi baseplates with the same chemical composition. A superelastic NiTi stent with 0.05 mm strut thickness was used as the control.

B. Additive manufacturing of the samples

An industrial LPBF system (Renishaw AM250, Stone, UK) was used for this work. The system is equipped with a 200 W single-mode fiber laser (R4, SPI, Southampton, UK) with 1070 nm wavelength and an optical chain that provides a 75 μm beam diameter in the focus position. The laser source is run in a pulsed mode (PW) by power modulation to achieve μs-long pulses. The system works under a controlled atmosphere. Before the build process, the chamber is filled with Ar, with 15 mbar over-pressure, and during the process, the oxygen content is maintained below 1000 ppm. All the experiments were carried out without any preheating of the substrate. A reduced build volume (RBV) platform was installed in the LPBF system, which limits the build chamber to $78 \times 78 \times 50$ mm^3 while employing a limited quantity of powder (<3 kg). The melting of the powder bed was achieved by emitting a peak power (P_{peak}) at 100 W for a fixed pulse duration (t_{on}) at 50 μs. Layer thickness (l_z) was set equal to 30 μm. The focal position was set to have the minimum beam size on the powder bed surface ($f = 0$ mm). On a scanning line, points exposed to the laser were separated by a given point distance (d_p), while different scanning lines were at a given hatch distance (d_h), which were both fixed at 30 μm. Meander scan strategy was used in which the scanning lines are parallel and rectilinear segments.[17] The process parameters are summarized in Table I. The build jobs were prepared using MATERIALISE MAGICS software (Materialise NV, Leuven, Belgium), which allows to place components on the baseplate area, perform the slicing phase, and assign process parameters. The parts were loaded in the software environment in STL format. A dedicated mesh with 10 mm diameter and 0.1 mm thick cylindrical struts was designed to test the efficacy of the chemical etching (Fig. 1).

C. Postprocessing of the samples

Heat treatment was performed under vacuum and Ar atmosphere (SAES Getters SpA, Lainate, Italy). Temperature and holding time were 500 °C for 15 min, respectively. To improve the surface quality of LPBF processed samples, chemical etching was performed to remove sintered particles and the staircase effect. In addition to surface quality improvement, the finishing process allowed to decrease the strut thickness. A nitric-hydrofluoric acid solution was employed, with a composition of 7% hydrofluoric acid (HF), 43% nitric acid (HNO_3), and 50% distilled water (H_2O) at room temperature for 14 min.

TABLE I. Parameters employed for the LPBF of NiTi meshes.

Parameter	Value
Layer thickness, z (μm)	30
Focal position, f (mm)	0
Peak power, P_{peak} (W)	100
Point and hatch distance, $d_p = d_h$ (μm)	30
Pulse duration, t_{on} (μs)	50
Scanning strategy	Meander

D. Surface characterization

X-ray photoelectron spectroscopy (XPS) characterization was carried out to determine the elemental and chemical composition of the scaffold surfaces (Thermo Scientific ESCALAB 250xi). A survey spectrum was collected using a 500 μm × 500 μm spot size and a standard aluminium x-ray source from 0 to 1200 eV, with a step size of 0.80 eV and pass energy of 187.85 eV, to identify all elements present at the surface. High resolution spectra for C1 s, O1 s, Ni2p, and Ti 2p regions were scanned with a 0.1 eV step size. Spectra were analyzed using CASAXPS and were charge corrected to adventitious carbon at 248.8 eV. Elemental concentrations at the surface were determined with relative sensitivity factors provided in the CasaXPS "quantify" function and library.

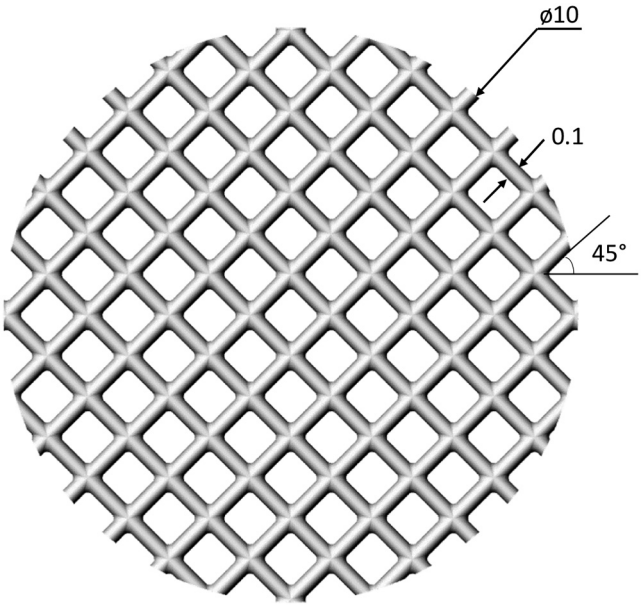

FIG. 1. NiTi mesh with thin struts produced by LPBF.

E. Biocompatibility testing

Two cell lines, the NCTC clone 929 (L929) and mouse macrophage cell line (RAW 264.7) was purchased from ATCC (Manassas, VA, USA). The cells used in experiments were thawed from cryopreservation and cultured in EMEM, 10% horse serum and 1% penicillin streptomycin for L929 cells and DMEM media (high glucose 4500 mg/l), 10% fetal bovine serum and 1% penicillin streptomycin for RAW 264.7 at 37 degrees Celsius (°C) and 5% CO_2. At passage 7, the cells were subcultured onto 96 well plates containing presterilized NiTi mesh and Nitinol stent materials at a seeding density of 1×10^5 cells per well. Cells cultured without NiTi metal materials were used as controls. After 24 h, a live-dead assay was carried out using 2 μM calcein-AM and 2 μg/ml ethidium bromide (Invitrogen Thermofisher Waltham, MA, USA), which stain live and dead cells, respectively. Hoechst dye at 10 μg/ml (Thermofisher, Waltham, MA, USA) was added to stain cell nuclei. The cells were incubated with the reagents in phosphate buffered saline (PBS) for 10 min in the dark at 37 °C and imaged using an Olympus fluorescent microscope. For evaluation of cytotoxicity, a lactate dehydrogenase (LDH) assay was used (Ab65393, ABCAM, USA). The protocol and analysis were determined using the manufacturer's instructions.

F. SEM image analysis of cells on scaffolds

Prior to cell culture experiments, the materials were cleaned in an ultrasonic bath containing acetone. This was followed by washes in 200 proof ethanol. The materials were air dried and imaged by scanning electron microscopy (Philips XL 40 ESEM). After the cell culture experiments, the materials were further assessed for cell attachment and spreading using field emission scanning electron microscopy (FE-SEM). Following 24-h incubation with the cells, the materials were fixed in 10% formalin and incubated for 2 days at 4 °C. The formalin was removed, and materials washed in PBS 3 times for 5-min intervals. Thereafter, serial dehydration was performed at increasing concentrations of ethanol (10, 30, 50, 70, 95, and 100%). Critical drying was also performed by adding hexamethyldisilazane (HMDS) and incubated for 30 min. The solution was removed and stored in a desiccator prior to SEM imaging.

G. Statistical analysis

The data were uploaded into Graphpad Prism (v9.3.0) for analysis. An unpaired Student's *T*-test with Welch's Correction for samples of unequal variance was used to test for statistical

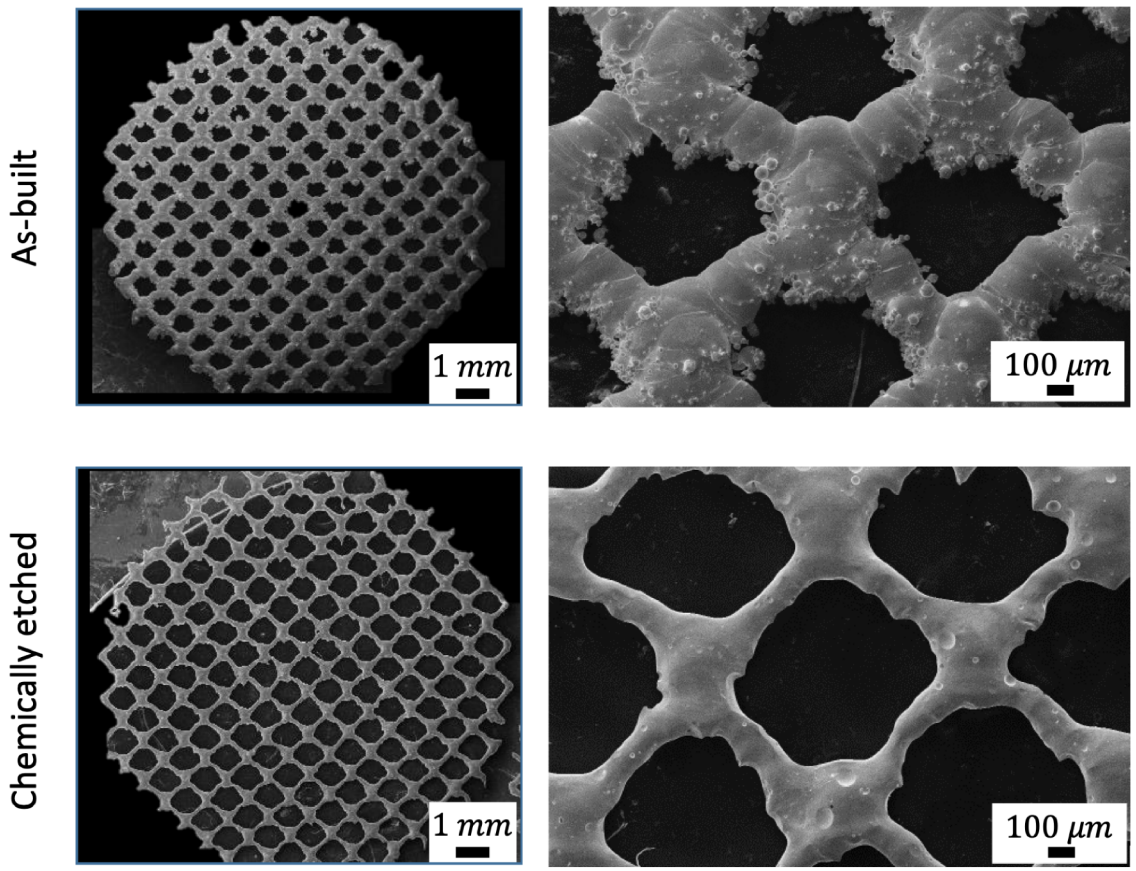

FIG. 2. SEM micrographs of the surfaces in as-built and chemically etched conditions. The build direction is vertically oriented with respect to the image plane.

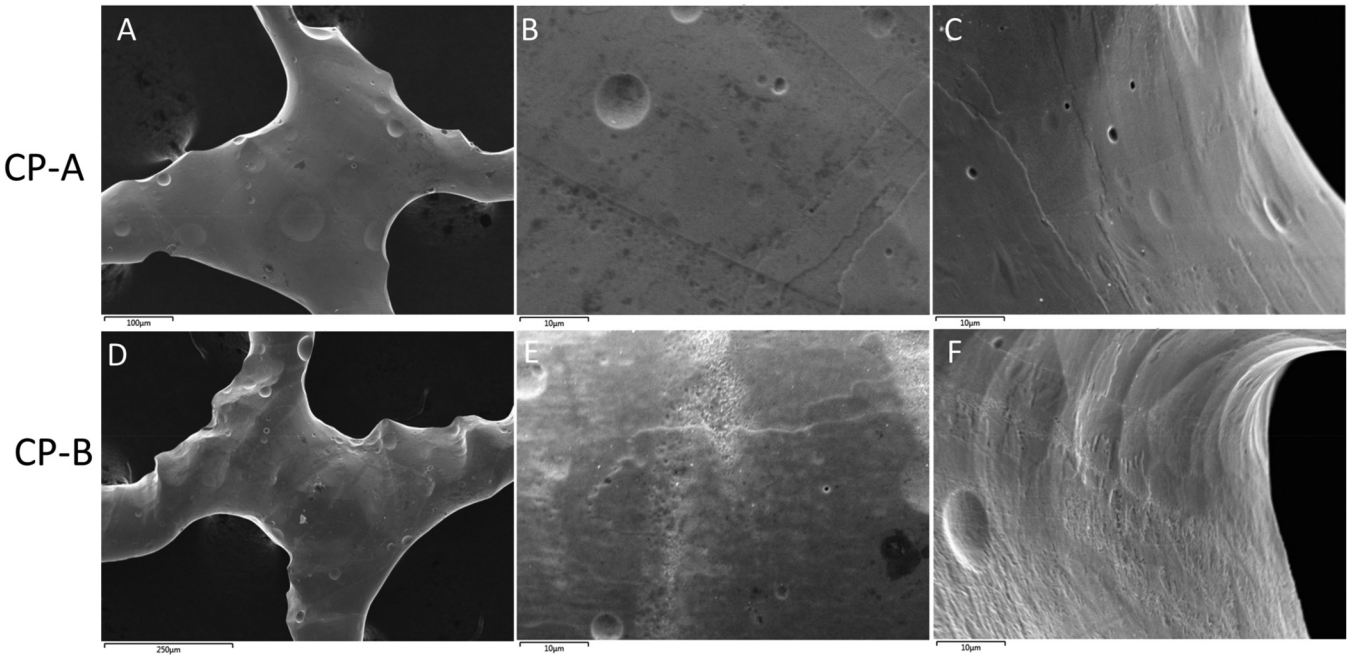

FIG. 3. SEM micrographs of the surfaces for the two scaffold conditions. (a)–(c) Represent low and high magnification images of the surface for the CP-A scaffolds, while (d)–(f) show low and high magnification for the CP-B scaffolds.

significance at $^{*}P < 0.01$. Graphs are presented as means and error bars are ± standard deviation.

III. RESULTS AND DISCUSSION

A. Additively manufactured NiTi mesh surface quality and material properties

1. Mesh geometry

Figure 2 shows the produced mesh in as-built and chemically etched conditions. In the as-built condition, the surface is composed of sintered particles and stratification lines along the build direction. The downfacing regions show sagging behavior due to the reduced heat transfer causing the enlargement of melt pool.[18] After chemical etching, the surfaces are free of sintered particles, and stratification in the form of the staircase effect is more visible.[19] On the other hand, the strut size is significantly reduced after the chemical etching phase. The strut diameter in as-built condition was 278 ± 37 μm, and 121 ± 12 μm after chemical etching.

2. Mesh surface chemistry

While the surface conditions and strut sizes were consistent throughout the produced specimens, different surface colourization was observed. The scaffolds were separated into two distinct groups that possessed consistent features. Samples that had a shiny metallic luster were separated into the "A" group, while samples that were darker, and presented a matte finish were categorized into the "B" group. Herein, the scaffolds will be reported as determined by their group designation, either chemically polished A (CP-A) or chemically polished B (CP-B). When evaluated microscopically, microtopographical features between CP-A and CP-B appear to be similar [Figs. 3(a)–3(e)]. We concluded that the differences in surface presentation were likely due to a difference in the optical properties of a chemically discrete surface oxide film on CP-B.[20]

We used XPS in order to determine the surface chemistry of the meshes from each group. Survey scans reveal the presence of oxygen (O1s), carbon (C1s), nitrogen (N1s), chlorine (Cl2p), phosphorous (P2p), silicon (Si2p), nickel (Ni2p), and titanium (Ti2p), for both scaffolds in CP-A and CP-B. A distinctive difference observed in CP-B was the presence of fluorine (2.59 at. %), which is likely sourced from the chemical polishing solution,[21] while it was not present on scaffolds in group CP-A. High resolution scans of the Ni2p, Ti2p, and O1s regions were performed to identify more species contributing to the surface presentation.

Atomic % of each element was calculated from survey scans using relative sensitivity factors within Casa. CP-A possessed significantly less Ni at the surface (0.19 at. %) than the CP-B group (3.30 at. %), shown in Figs. 4(a) and 4(e). The Ni2p region displays a complex peak regime which includes metal oxide and satellite contributions. The Ni2p3/2 peak is present in both groups around 857 eV, and the Ni 2p1/2 peak is present near 875 eV. Ni (metallic) peaks are found at 852 eV, which were not present in either group [Fig. 4(b)]. This suggests the entire form of Ni at the surface is bound as an oxide. The peak found at 857 eV was determined to originate from NiOOH. Cp-A has an additional large contribution from NiO (855 eV), which is not present for CP-B. Conversely,

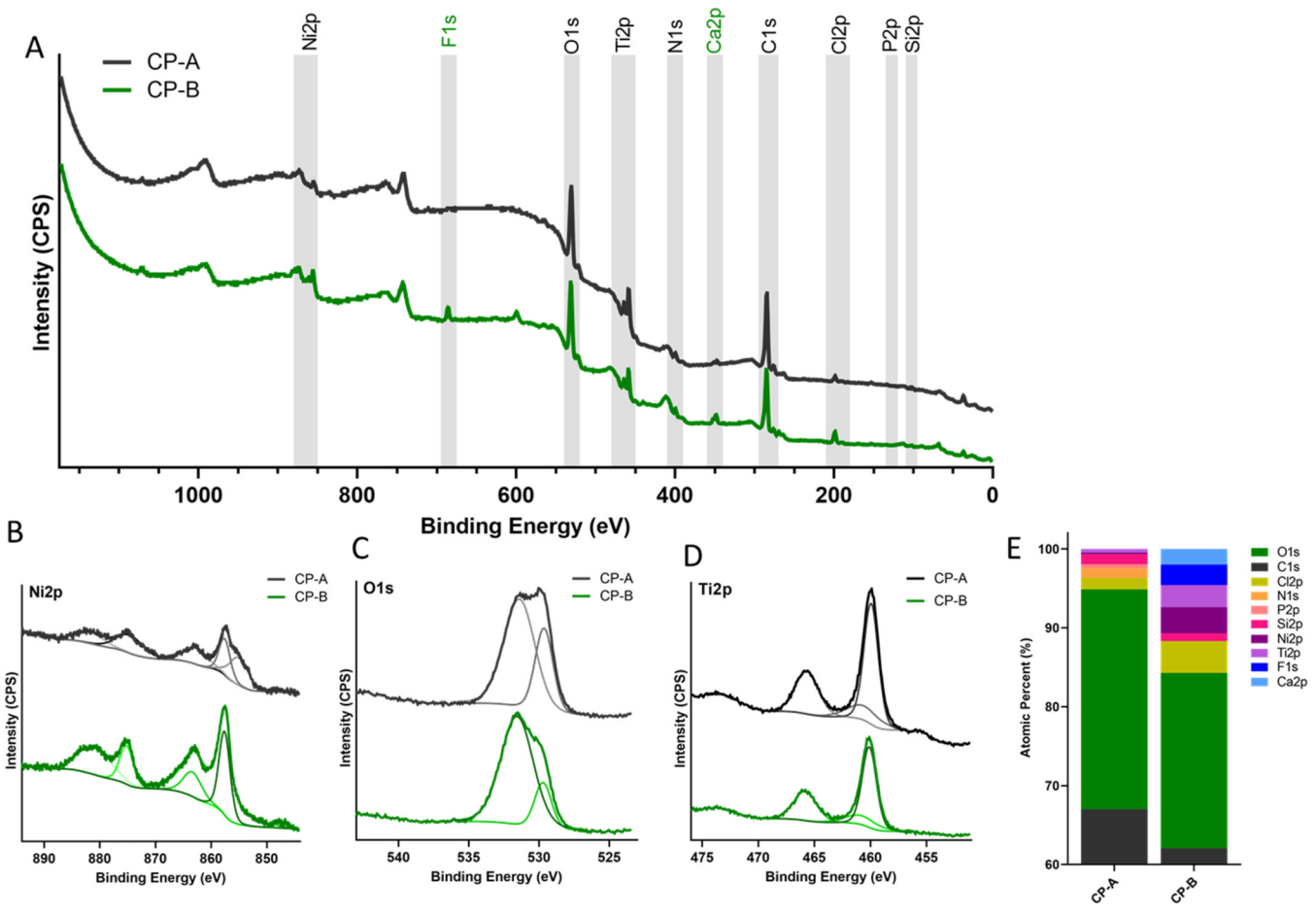

FIG. 4. XPS characterization of representative meshes from the two groups. (a) Survey scans for CP-A and CP-B, (b)–(d) are high resolution scans of the Ni 2p, O1s, and Ti2p regions, respectively, and (e) shows at. % calculation from the survey scans for the two conditions.

CP-B possesses a large contribution from $Ni(OH)_2$ that is not present for CP-A [Fig. 4(b)].

High resolution scans of the Ti 2p region for both the CP-A and CP-B groups in Fig. 4(d) do not show distinctive chemical shifts in the primary TiO_2 peaks (460 eV). No metallic Ti peak was observed, suggesting all Ti is bound in the oxide form, and the binding energy of the Ti 3/2p and Ti 1/2p regions are not shifted. The O1s region showed distinctive changes between the CP-A and CP-B groups [Fig. 4(c)]. The two primary components that were fit are attributed to NiOx/TiOx and NiOx(OH)y configurations. CP-B has a higher component contribution from its NiOx(OH)y group at 531.5 eV (81.5 at. %), while CP-A shows a more pronounced NiOx peak (31.43 at. %). This corresponds with the findings in the Ni 2p region.

B. Biological performance

1. Cell viability

We wanted to visualize the spreading of fibroblasts (L929) and macrophage cells (RAW 264.7) onto the LPBF produced scaffolds with respect to an industry standard. Figure 5 shows spreading of both cell types onto the CP-A condition, with minimal spreading or cells present on CP-B. There is a morphological change and increase in the cell attachment phenomena between the NiTi stent and the CP-A group, which could be attributed toward a difference in surface features.[22]

Our live dead staining revealed significant toxicity and reduced cellular attachment for the CP-B group. Figure 6 shows the reduced amount of Hoechst and Calcein signal from CP-A to CP-B. The high magnification frames shown displays representative images at scaffold strut crossings. Large cell attachment with mild death is seen for the control stent material and CP-A, while little cellular attachment is seen for CP-B. This discrepancy is quantified in panel A, which shows the average live cells per imaging frame for CP-A vs CP-B. Due to large differences in surface area, the NiTi stent control is not presented. CP-A possessed on average 500.2 cells/frame ± 136, while CP-B showed a statistically significant reduction in live cells on the scaffold (153.7 ± 100.8, $P < 0.01$).

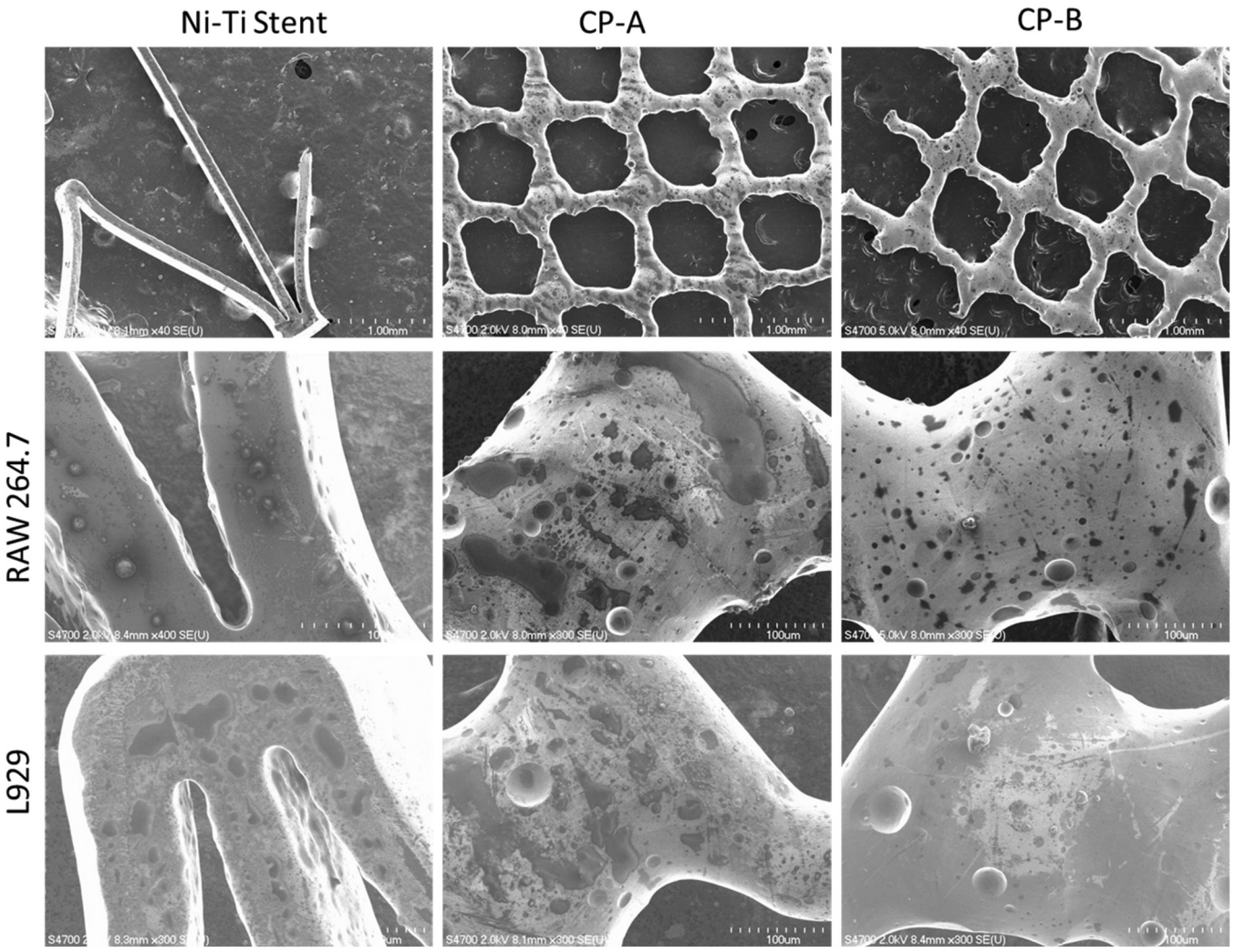

FIG. 5. Cell spreading onto NiTi scaffolds visualized by FE-SEM. Low magnification scale bar is 1 mm and high magnification scale bar is 100 μm.

The reduction in live cells that attached to the scaffolds does not allude to toxicity per se, so we employed an LDH assay in order to quantify material induced cellular death. LDH is a stable intracellular enzyme which is rapidly released into the cell culture medium upon damage of the plasma membrane. The LDH released from the cells oxidizes lactate to generate NADH, which then reacts with an assay reagent WST to generate a yellow color that can be measured spectrophotometrically. The color intensity correlates directly with the number of damaged cells. When normalized to cells incubated with a lysis agent, the NiTi stent and CP-A materials induced minimal cell lysis ($8.6 \pm 8.74\%$ vs $0.125 \pm 3.4\%$, respectively). In contrast, the CP-B material induced a relatively large amount of cell lysis ($20.9 \pm 5.1\%$), which was significantly increased when compared to CP-A ($P < 0.01$).

The overall results indicate the influence of variable outcomes during the finishing operations involved in the additive manufacturing process chain. It is confirmed that through the correct control of the chemical etching process a biocompatible surface performance can be achieved. On the other hand, process variations induced by the saturation of the employed chemical etchant, local temperature variations, contaminations may lead to inadequate biocompatibility. Such issues may be present in biomedical device manufacturing as well as electronics where similar processes are commonly applied.[23] The distinct surface features, topography, and chemistry of additively manufactured products can indeed render them different from more conventional cast, drawn, or laser cut products.[24] In industrial practice, the processing conditions can be stabilized via continuous monitoring of the process variables.

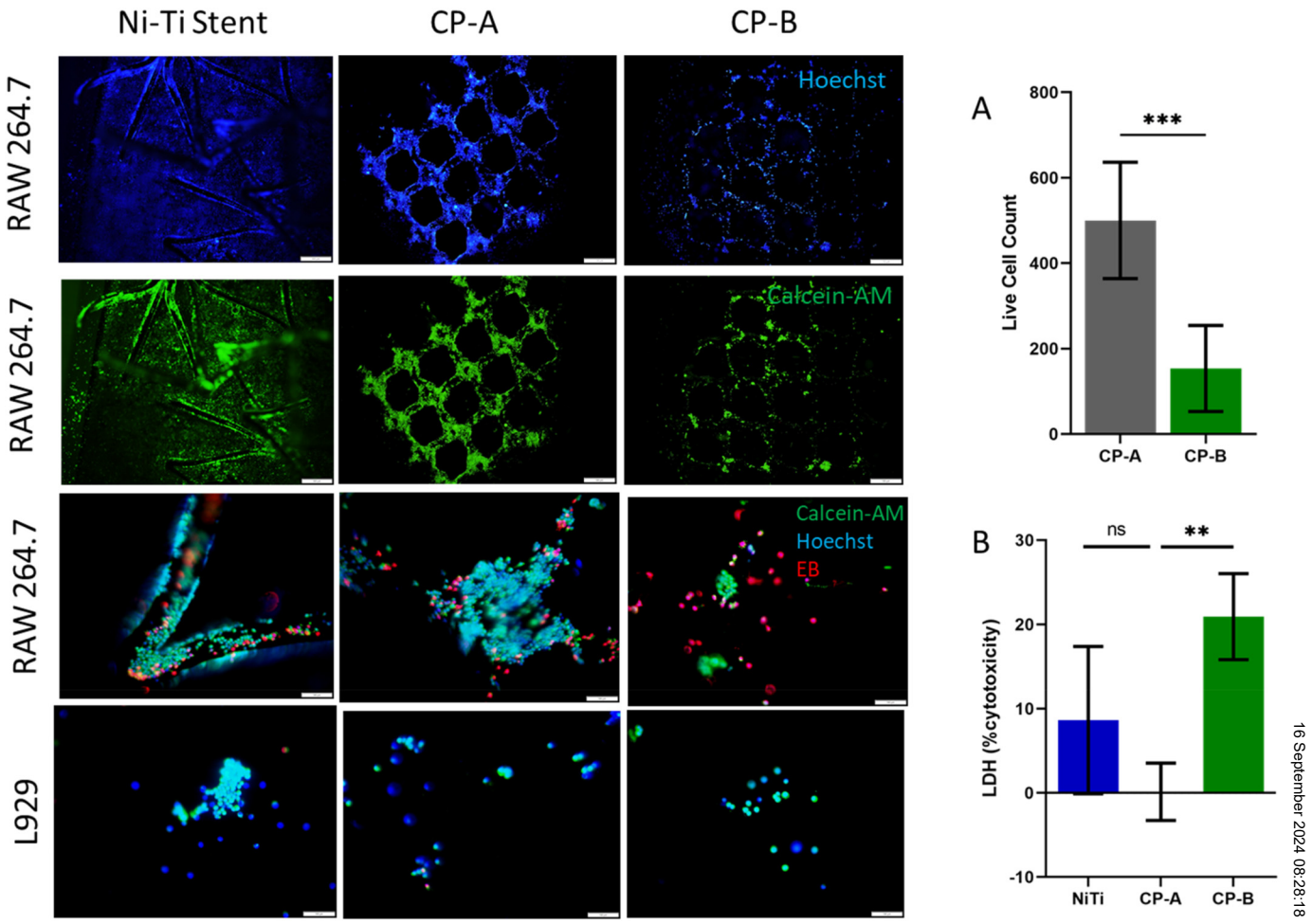

FIG. 6. Live dead staining of cells incubated onto control and experimental scaffolds. Panel (a) shows RAW264.7 live cells counted by frame, while panel (b) presents results from the LDH assay. EB, ethidium bromide. Scale bar is100 μm.

IV. CONCLUSIONS

It is currently accepted that conventionally processed and additively manufactured NiTi materials will have to undergo surface treatments in order to be implant ready for biomedical applications. The surface treatments include mechanical and/or chemical methods, aim to reduce roughness, surface impurities, and increase the corrosion resistance of the material. We sought to test the biocompatibility of our scaffolds after a chemical etching procedure that was effective at minimizing the topographical landscape of the scaffolds after manufacturing (Fig. 2). Although two distinct oxide films were created in the process (labeled CP-A and CP-B), no qualitative changes in microroughness were seen between the two conditions (Fig. 3). This allows us to draw conclusions about our biocompatibility assay results as a function of the oxide film. Future practices of manufacturing NiTi scaffolds using LPBF should focus on producing surface films that are not only smooth, but free of cytotoxic Ni based oxides.

ACKNOWLEDGMENTS

The authors acknowledge support of Valentina Finazzi during the specimen preparation. Parts of this study were completed using Michigan Technological University's Applied Chemical and Morphological Analysis Laboratory. We would like to acknowledge Margaret E. Plank for assisting and performing cell culture experiments. We would also like to thank Zachary Alesch for his contributions on SEM imaging and sample preparation.

AUTHOR DECLARATIONS

Conflict of Interest

The authors have no conflicts to disclose.

Ethics Approval

The research work presented did not involve any animal or human experimental studies.

Author Contributions

Maria P. Kwesiga: Data curation (equal); Formal analysis (equal); Investigation (equal); Writing – original draft (equal); Writing – review & editing (equal). **Roger J. Guillory:** Conceptualization (equal); Data curation (equal); Formal analysis (equal); Investigation (equal); Methodology (equal); Resources (equal); Supervision (equal); Writing – original draft (equal); Writing – review & editing (equal). **Ali Gökhan Demir:** Conceptualization (equal); Formal analysis (equal); Investigation (equal); Methodology (equal); Resources (equal); Supervision (equal); Writing – original draft (equal); Writing – review & editing (equal).

DATA AVAILABILITY

The data that support the findings of this study are available from corresponding author upon reasonable request.

REFERENCES

[1]K. Safaei *et al.*, JOM **73**, 3771 (2021).
[2]V. Finazzi, F. Berti, R. J. Guillory, II, L. Petrini, B. Previtali, and A. G. Demir, Procedia CIRP **110**, 242 (2022).
[3]S. Dadbakhsh, M. Speirs, J. Van Humbeeck, and J. P. Kruth, MRS Bull. **41**, 765 (2016).
[4]F. S. L. Bobbert, K. Lietaert, A. A. Eftekhari, B. Pouran, S. M. Ahmadi, H. Weinans, and A. A. Zadpoor, Acta Biomater. **53**, 572 (2017).
[5]M. Taheri Andani *et al.*, J. Intell. Mater. Syst. Struct. **27**, 2661 (2016).
[6]A. Fischer, O. Thomusch, S. Benz, E. Von Dobschuetz, P. Baier, and U. T. Hopt, Ann. Thorac. Surg. **81**, 467 (2006).
[7]C. J. Pan, H. Q. Liu, Y. N. Wang, and H. Y. Ding, Mater. Res. Bull. **60**, 217 (2014).
[8]S. Kujala, J. Ryhänen, A. Danilov, and J. Tuukkanen, Biomaterials **24**, 4691 (2003).
[9]S. Maffia, V. Finazzi, F. Berti, F. Migliavacca, L. Petrini, B. Previtali, and A. G. Demir, Smart Mater. Struct. **30**, 105010 (2021).
[10]Z. Xiong *et al.*, Addit. Manuf. **57**, 102960 (2022).
[11]L. Petrini and F. Migliavacca, J. Metall. **2011**, 1 (2011).
[12]S. Trigwell, R. D. Hayden, K. F. Nelson, and G. Selvaduray, Surf. Interface Anal. **26**, 483 (1998).
[13]G. Mani, D. Porter, K. Grove, S. Collins, A. Ornberg, and R. Shulfer, J. Biomed. Mater. Res., Part B **110**, 2763 (2022).
[14]H. Zhao, J. Van Humbeeck, J. Sohier, and I. De Scheerder, J. Mater. Sci. Mater. Med. **13**, 911 (2002).
[15]A. G. Demir and B. Previtali, Mater. Des. **119**, 338 (2017).
[16]J. X. Liu, D. Z. Yang, F. Shi, and Y. J. Cai, Thin Solid Films **429**, 225 (2003).
[17]V. Finazzi, A. G. Demir, C. A. Biffi, F. Migliavacca, L. Petrini, and B. Previtali, J. Manuf. Process. **55**, 161 (2020).
[18]A. Triantaphyllou, C. L. Giusca, G. D. Macaulay, F. Roerig, M. Hoebel, R. K. Leach, B. Tomita, and K. A. Milne, Surf. Topogr.: Metrol. Prop. **3**, 024002 (2015).
[19]M. Speirs, B. Van Hooreweder, J. Van Humbeeck, and J. P. Kruth, J. Mech. Behav. Biomed. Mater. **70**, 53 (2017).
[20]C. W. Ng, A. S. Mahmud, M. N. Ahmad, M. F. Razali, and Y. Liu, Materialwiss. Werkstofftech. **53**, 47 (2022).
[21]C. Y. Zheng, F. L. Nie, Y. F. Zheng, Y. Cheng, S. C. Wei, and R. Z. Valiev, Appl. Surf. Sci. **257**, 9086 (2011).
[22]M. Es-Souni, M. Es-Souni, and H. Fischer-Brandies, Biomaterials **23**, 2887 (2002).
[23]J. Lorenz, E. Bär, S. Barraud, A. R. Brown, P. Evanschitzky, F. Klüpfel, and L. Wang, Micromachines **10**, 6 (2019).
[24]M. Anilli, A. G. Demir, and B. Previtali, Rapid Prototyp. J. **24**, 562 (2018).